available at www.sciencedirect.com

ScienceDirect

journal homepage: www.elsevier.com/locate/chnjc

Article

Low temperature CO oxidation on Ni-promoted CuO-CeO_2 catalysts

CHEN Guoxing [a], LI Qiaoling [a], WEI Yucai [a], FANG Weiping [a,b], YANG Yiquan [a,b,*]

[a] *Department of Chemical and Biochemical Engineering, College of Chemistry and Chemical Engineering, Xiamen University, Xiamen 361005, Fujian, China*
[b] *Department of Chemistry, College of Chemistry and Chemical Engineering and National Engineering Laboratory for Green Chemical Production of Alcohols, Ethers and Esters, Xiamen University, Xiamen 361005, Fujian, China*

ARTICLE INFO

Article history:
Received 5 September 2012
Accepted 11 October 2012
Published 20 February 2013

Keywords:
Copper
Cerium
Carbon monoxide
Oxidation
Nickel
Solid solution

ABSTRACT

A series of $Ce_{20}Cu_5Ni_yO_x$ catalysts for CO oxidation at low temperature were prepared and characterized by N_2 adsorption, X-ray diffraction, temperature-program reduction by H_2, X-ray photoelectron spectroscopy (XPS), and Raman spectroscopy. $Ce_{20}Cu_5Ni_{0.4}O_x$ exhibited the highest catalytic activity. The addition of NiO increased the amount of copper ions doped into the CeO_2 matrix and gave more oxygen vacancies in ceria by the formation of a Ni-O-Ce solid solution. XPS results showed that large quantities of Cu^+, Ce^{3+}, and lattice oxygen existed in the fresh $Ce_{20}Cu_5Ni_{0.4}O_x$ catalyst. Cu^+ ions in the catalyst can easily migrate to the ceria lattice to form a Cu-O-Ce solid solution, which enhanced the release of the lattice oxygen of the oxides under a reducing atmosphere. The high catalytic activity of $Ce_{20}Cu_5Ni_{0.4}O_x$ is due to the promoter giving increased amounts of Cu^+ in the catalyst and the formation of solid solutions of both Cu-O-Ce and Ni-O-Ce.

1. Introduction

In recent years, increasing attention has been focused on the catalytic oxidation of carbon monoxide at ambient temperature due to its important applications in mine rescue devices for human safety, carbon dioxide lasers, proton exchange membrane fuel cells as well as many other applications in air purification devices, CO sensors, and even the burning of a cigarette [1–4]. In addition, CO oxidation is an elementary step in many important industrial processes such as the production of methanol and the water-gas shift reaction [5,6]. Although the kinetics and mechanism of CO oxidation to CO_2 have been investigated by many researchers [1,7–9], many features of it are not yet fully understood.

Precious metal catalysts based on supported gold have been widely used for the low temperature oxidation of CO with the precious metal deposited as nanoparticles on metal oxides [10–13]. However, the limited availability and high cost of precious metals have long motivated the search for substitute catalysts and the development of non-noble metal catalysts [14,15]. Metal-ceria systems are several orders of magnitude more active than other oxide supported catalysts for various redox reactions because of the high oxygen storage capacity and reducibility of ceria. The CuO/CeO_2 system is a promising catalyst for CO oxidation [7,16–20], because it has a specific activity that is several orders of magnitude higher than that of conventional Cu-based catalysts and which is comparable or even superior to the activity of Pt-based catalysts. The role of ceria as a support for non-noble metals is based on its oxygen storage capacity and also its ability to improve the dispersion of the non-noble metal active ingredients. The high mobility of its lattice oxygen and the redox property of ceria are generally regarded as playing key roles in governing the catalytic behavior. The oxygen storage capacity of ceria and catalytic activity of Cu-Ce catalysts can be improved by doping with zirconium, which can form a CeO_2-ZrO_2 solid solution and restrain the growth of CeO_2 crys-

* Corresponding author. Tel.: +86-592-2186368; Fax: +86-592-2180361; E-mail: yyiquan@xmu.edu.cn
This work was supported by the China Tobacco Fujian Industrial Corporation.
DOI: 10.1016/S1872-2067(11)60468-3 | http://www.sciencedirect.com/science/journal/18722067 | Chin. J. Catal., Vol. 34, No. 2, February 2013

tallites [21–23]. However, little attention has been given to the influence of Ni doping on the performance of a CuO-CeO_2 catalyst.

In CeO_2, the facile Ce^{4+}/Ce^{3+} redox couple gives a high oxygen storage capacity (OSC) by the reversible addition and removal of oxygen in the fluorite structure of ceria. It has been observed that the redox property of $Ce_{1-x}MO_y$ solid solutions formed by incorporating other metal ions into CeO_2 is better than that of CeO_2 alone. This suggested the use of Ni^{2+} cations with a smaller size that can be incorporated into the cubic lattice to form a solid solution and help the change of Ce^{4+} to Ce^{3+}. In addition, it is also possible that Cu ions can have a more facile redox behavior during oxidation and reduction oscillations from the introduction of NiO.

In the present work, $Ce_{20}Cu_5Ni_yO_x$ catalysts with various nickel loadings (y = 0, 0.4, 5) were prepared by the reverse co-precipitation method. The copper species of the catalysts were studied by electron spin resonance (EPR) and X-ray photoelectron spectroscopy (XPS). NiO promotion of the formation of these Cu-promoting species was further discussed using X-ray diffraction (XRD) and Raman characterization data.

2. Experimental

2.1. Catalyst preparation

$Ce_{20}Cu_5Ni_yO_x$ catalysts with different nickel contents were prepared by the reverse co-precipitation method. $Cu(NO_3)_2{\cdot}3H_2O$, $Ce(NO_3)_3{\cdot}6H_2O$, and $Ni(NO_3)_2{\cdot}6H_2O$ were used as sources of Cu, Ce, and Ni, respectively. A mixed solution of weighed quantities of copper nitrate, cerium nitrate, and nickel nitrate was added to a solution of sodium hydroxide at a rate of 3–4 ml/min under vigorous stirring at 60 °C. The pH value was adjusted to 9.7–10 with sodium hydroxide to produce a precipitate suspension. Then, a small amount of L-glutamate surfactant was added to the suspension after 5 min. The precipitate obtained was aged at 60 °C for one hour under stirring and then filtered and washed with hot distilled water several times to remove excess ions, followed by drying at 110 °C for 4 h. The dried material was crushed and calcined in air at 350 °C for 3 h to give the final powder $Ce_{20}Cu_5Ni_yO_x$ catalyst. A $Ce_{20}Cu_5O_x$ sample was prepared by the same method as a reference.

2.2. Catalytic activity measurement

The activity of the catalyst was tested in a quartz tubular fixed-bed reactor with 0.2 g of catalyst. The reaction temperature ranged from 40 to 120 °C. The total feed gas flow rate was 60 ml/min, corresponding to a gas hourly space velocity (GHSV) of 18000 h^{-1}. The composition of the feed gas was 1% CO, 1% O_2, and 98% N_2. The product was analyzed by an online gas chromatograph equipped with a carbon molecular sieve column (1 m × 3 mm) and a 5A molecular sieve column (2 m × 3 mm) connected in parallel and a thermal conductivity detector.

2.3. Catalyst characterization

The specific surface area, pore volume, and pore diameter were determined by the BET method on a Quantachrome Autosorb-1 instrument at –196 °C with N_2 adsorbent. Powder XRD patterns were measured on a Panalytical X'Pert PRO X-ray diffractometer using Cu $K_{\alpha1}$ radiation. The XRD patterns were referenced to powder diffraction files (ICDD-FDP data base) for identification. Visible Raman spectra were recorded on a computer-controlled Renishaw Invia spectrometer system using a 532 nm argon ion laser beam as exciting source. The spectra resolution was 2 cm^{-1} and the laser power was 20 mW. All Raman spectra were recorded under ambient conditions. UV Raman spectra were recorded on a UV Raman spectrograph using a 325 nm argon ion laser beam as exciting source. The laser power was below 4.0 mW for the 325 nm radiation. All the UV Raman spectra were also recorded at room temperature.

XPS characterization was performed on a PHI-Quantum 2000 spectrometer. The sample powder was pressed into a wafer for the analysis. The C 1*s* line (284.6 eV) of adventitious carbon was used as the reference to calibrate the binding energy (BE). Temperature-programmed reduction (H_2-TPR) measurement was carried out on a quartz reactor. After treatment at 300 °C in Ar for 1 h, the sample was cooled to room temperature in the same atmosphere, and then the gas was switched to a mixed gas of 5%H_2-95%N_2 at a rate of 30 ml/min. When there was a stable baseline, the sample was heated at a rate of 10 °C/min in 5%H_2-95%N_2. The spectra were recorded after the reaction reached steady state.

3. Results and discussion

3.1. Textural characterization results

Table 1 lists the surface texture data of the support and catalysts obtained from N_2 adsorption measurements. As compared with the pure CeO_2, after loading of copper, the specific surface area and pore volume of $Ce_{20}Cu_5O_x$ were increased from 86 m^2/g and 0.121 cm^3/g to 135.1 m^2/g and 0.184 cm^3/g, respectively. The $Ce_{20}Cu_5Ni_{0.4}O_x$ catalyst with a small amount of Ni had a similar pore volume and average pore diameter to $Ce_{20}Cu_5O_x$, but had a higher specific surface area. The $Ce_{20}Cu_5Ni_5O_x$ catalyst with a high loading of Ni had the smaller specific surface area (125.5 m^2/g), pore volume (0.117 cm^3/g), and average pore diameter (3.73 nm). These were ascribed to the existence of some CeO_2 crystallites surrounded by small NiO crystallites, leading to fewer pores and hence a smaller specific surface area.

The N_2 adsorption isotherms and pore diameter distribution curves of the catalysts are shown in Fig. 1. All isotherms were typical Type IV curves, which are characteristic of mesoporous

Table 1
Surface texture of the support and catalysts.

Sample	Surface area (m_2/g)	Pore volume (cm_3/g)	Average pore diameter (nm)
CeO_2	86.0	0.121	7.30
$Ce_{20}Cu_5O_x$	135.1	0.184	5.45
$Ce_{20}Cu_5Ni_{0.4}O_x$	142.2	0.178	4.99
$Ce_{20}Cu_5Ni_5O_x$	125.5	0.117	3.73

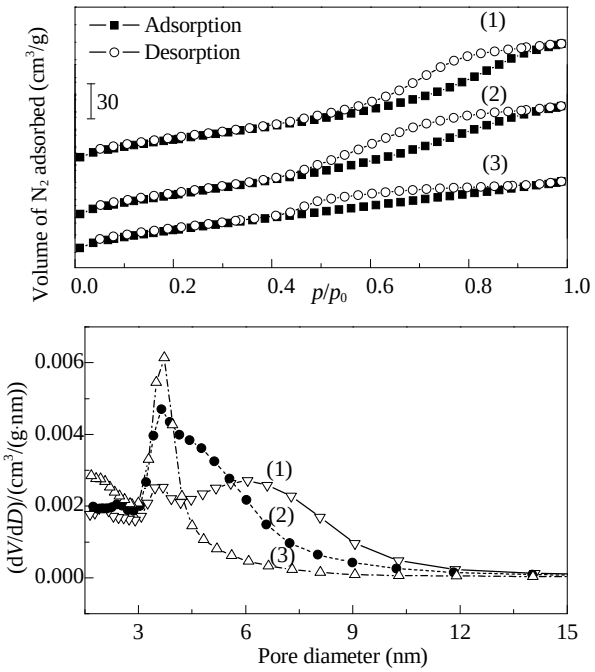

Fig. 1. N_2 adsorption-desorption isotherms and pore size distribution of the catalysts. (1) $Ce_{20}Cu_5O_x$; (2) $Ce_{20}Cu_5Ni_{0.4}O_x$; (3) $Ce_{20}Cu_5Ni_5O_x$.

materials, with the H_2 hysteresis loop. The observed isotherms indicated ink bottle-type pores with narrow orifices and a broader interior. The capillary condensation step for the $Ce_{20}Cu_5Ni_{0.4}O_x$ sample was shifted to a lower relative pressure in comparison to that of the $Ce_{20}Cu_5O_x$ catalyst without NiO addition, which indicated a smaller mesopore size of the ceria powder. Moreover, the condensation step for all the catalysts was very steep, indicating a highly uniform distribution of the pore size and good pore connectivity [24]. The pore diameter distribution was calculated from the adsorption branch of the isotherms using the BJH algorithm. The peak of the pore diameter distribution for $Ce_{20}Cu_5Ni_{0.4}O_x$ was slightly narrower and was shifted towards the left in comparison with that from the $Ce_{20}Cu_5O_x$ catalyst, indicating a decrease in pore diameter. When the nickel loading was high, the peaks were obviously narrower and tiny pores with diameters of 1.5–3 nm appeared. Nickel and copper cannot enter the small diameter pores, but existed at the mouth, which caused the mouths of the smaller pores to be closed due to the blocking by nickel ions. This may be the reason why the BET surface area and pore volume for the $Ce_{20}Cu_5Ni_5O_x$ catalyst decreased. This result indicated that a small nickel loading has a positive effect on the increase of the surface area of a CuO-CeO_2 catalyst and made the mesopore size of the ceria smaller. To explore what happened after the introduction of NiO, further investigations on the catalysts were performed, as discussed below.

3.2. XRD results

Figure 2 shows the XRD patterns of CeO_2 and the $Ce_{20}Cu_5Ni_yO_x$ catalysts with different nickel loading. As can be seen from Fig. 2, peaks that can be ascribed to CeO_2 with a fluorite structure appeared for all the catalysts. No diffraction

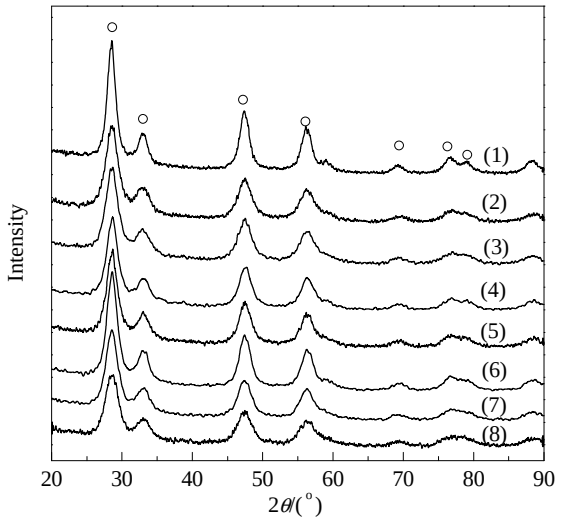

Fig. 2. XRD patterns of the CeO_2 support and the catalysts. (1) CeO_2; (2) $Ce_{20}Cu_5O_x$; (3) $Ce_{20}Cu_5Ni_{0.2}O_x$; (4) $Ce_{20}Cu_5Ni_{0.3}O_x$; (5) $Ce_{20}Cu_5Ni_{0.4}O_x$; (6) $Ce_{20}Cu_5Ni_{0.5}O_x$; (7) $Ce_{20}Cu_5Ni_{2.5}O_x$; (8) $Ce_{20}Cu_5Ni_5O_x$.

peak corresponding to CuO (2θ = 35.6°, 38.8°, 61.5°) was detected, suggesting that the Cu species were highly dispersed on the surface of the ceria support and produced various surface Cu^{2+} species and clusters, and some Cu ions may be incorporated into the CeO_2 lattice. The Ni^{2+} ion (2θ = 37°, 44.3°, 62.9°) peaks were also not detected by XRD. The existence of isolated surface Cu^{2+} clusters were confirmed by the hyperfine structure in EPR spectrum [14,15]. Note that the Cu^{2+} ionic radius (0.072 nm) is smaller than that of Ce^{4+} (0.092 nm). The lattice parameter from the XRD data also indicated that it is possible for some Cu^{2+} ions to be incorporated into the cubic lattice to form homogeneous Cu-Ce-O solid solutions.

3.3. Raman spectra

Figure 3 shows the visible Raman spectra of the $Ce_{20}Cu_5Ni_yO_x$ catalysts with different nickel loadings and the reference samples (CeO_2 and $Ce_{20}Cu_5O_x$). It can be seen from

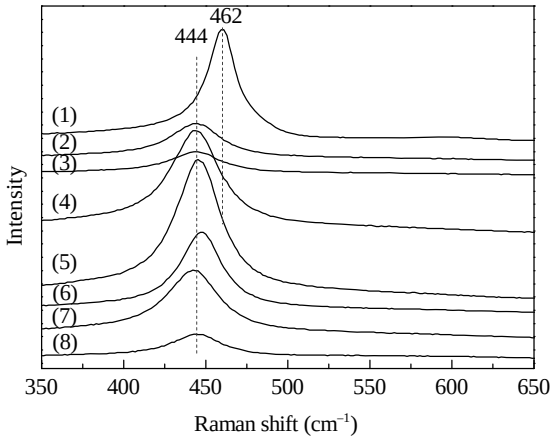

Fig. 3. Visible raman spectra of the support and the catalysts excited by 532-nm laser. (1) CeO_2; (2) $Ce_{20}Cu_5O_x$; (3) $Ce_{20}Cu_5Ni_{0.2}O_x$; (4) $Ce_{20}Cu_5Ni_{0.3}O_x$; (5) $Ce_{20}Cu_5Ni_{0.4}O_x$; (6) $Ce_{20}Cu_5Ni_{0.5}O_x$; (7) $Ce_{20}Cu_5Ni_{2.5}O_x$; (8) $Ce_{20}Cu_5Ni_5O_x$.

Fig. 3 that a Raman active band at 462 cm^{-1} due to cubic CeO_2 was observed, while the peak at 462 cm^{-1} was shifted to 444 cm^{-1} for the catalysts. The peak shift indicated a change in the lattice parameters [27], which was inconsistent with the lattice parameters deduced from the XRD characterization results. The most probable interpretation for the shift and broadening of the peaks is the presence of oxygen vacancies, corresponding to a stoichiometry of CeO_{2-x}, which suggested the formation of Cu-Ce-O solid solutions [28]. It is known that the substitution of Cu^{2+} for Ce^{4+} would generate oxygen vacancies around Cu^{2+}-O-Ce^{4+} (denoted as *-Cu^{2+}-O-Ce^{4+}, the symbol * represents an oxygen vacancy) in order to maintain charge neutrality [29]. As can be seen from Fig. 3, the peak at 444 cm^{-1} became broader and stronger with increasing nickel content. It was strongest when the Cu/Ni atomic ratio was 5:0.4. The peak at 444 cm^{-1} became broader and weaker after the introduction of too much Ni and became just like that from $Ce_{20}Cu_5O_x$. We did not find the bands at 552 and 631 cm^{-1} for NiO species [30]. This may mean that the substitution of Ni^{2+} for Ce^{4+} inside the CeO_2 structure to form a solid solution occurred.

Figure 4 shows the UV Raman spectra of the $Ce_{20}Cu_5Ni_yO_x$ catalysts and the reference sample ($Ce_{20}Cu_5O_x$). For all the samples, a broad band with a relatively high intensity was observed at 432 cm^{-1}, which was due to cubic CeO_2, together with two bands at 597 and 1196 cm^{-1}, which are not normally observed in the Raman spectra. The band at 432 cm^{-1} was due to the F_{2g} vibrational mode typical of the cubic structure, and the bands at 597 and 1196 cm^{-1} were attributed to oxygen vacancies [28,31,32] generated as charge compensation for the defects induced by the incorporation of other metal cations into the ceria lattice. The band at 317 cm^{-1} is an indication of some distortion of the oxygen sublattice and can be attributed to the t'' phase [33]. This phase is a fluorite type cation sublattice with oxygen atoms displaced from the ideal fluorite sites to give a tetragonal phase [33]. In addition, we observed that the band at 802 cm^{-1} for the $Ce_{20}Cu_5O_x$ samples was very weak. The addition of Ni enhanced these Raman peaks, and a broad band at 802 cm^{-1} was observed for the $Ce_{20}Cu_5Ni_yO_x$ catalysts. The intensity of the band at 802 cm^{-1} due to $Ce_{20}Cu_5Ni_{0.4}O_x$ was the highest among the samples, which suggested a synergistic interaction among Ni-O, Cu-O, and Ce-O. We ascribed the interfacial metal oxide-support synergistic effect to the formation of a O-Cu^{2+}-Ce^{4+}-Ni^{2+}-O cluster. The synergistic effect of the copper, ceria, and Ni species is believed to be beneficial for CO oxidation. It should be kept in mind that the incorporation of metal cations into the ceria fluorite lattice must be accompanied by the formation of oxygen vacancies [34]. The presence of oxygen vacancies in all the samples indicated the formation of a solid solution between cerium oxide and the other oxide. As compared with the $Ce_{20}Cu_5O_x$ catalyst, the $Ce_{20}Cu_5Ni_yO_x$ catalysts with loaded nickel showed enhanced Raman peaks at 594 and 1196 cm^{-1}, indicating an increase in oxygen vacancies. Moreover, we observed that the relative amount of oxygen vacancies in the $Ce_{20}Cu_5Ni_{0.4}O_x$ catalyst was more than those for the other catalysts. This suggested the formation of a solid solution of Ce-Ni-O by the incorporation of Ni^{2+} ions into the ceria lattice. The $Ce_{20}Cu_5Ni_{0.4}O_x$ catalyst is in the form of an imperfect face centered cubic structure, which gave increased oxygen vacancies and the distortion of the lattice, and thus enhanced the oxygen storage/release performance of the catalyst. In addition, the peaks at 802 cm^{-1} for the $Ce_{20}Cu_5Ni_{0.4}O_x$ sample were stronger than those for the other samples, which suggested a change of the surface structure of ceria and the relatively free movement of oxygen atoms.

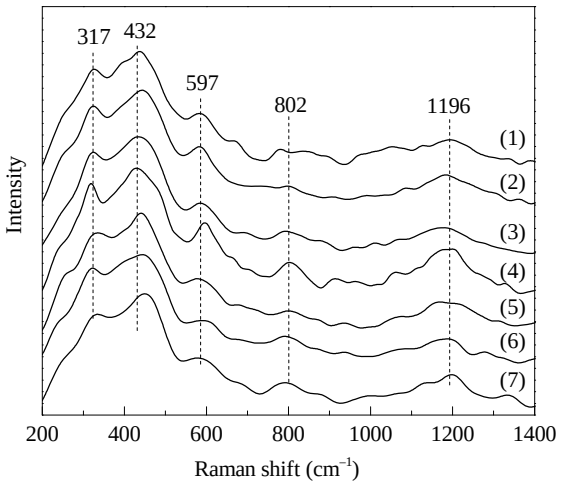

Fig. 4. UV Raman spectra of the catalysts excited by a 325-nm laser. (1) $Ce_{20}Cu_5O_x$; (2) $Ce_{20}Cu_5Ni_{0.2}O_x$; (3) $Ce_{20}Cu_5Ni_{0.3}O_x$; (4) $Ce_{20}Cu_5Ni_{0.4}O_x$; (5) $Ce_{20}Cu_5Ni_{0.5}O_x$; (6) $Ce_{20}Cu_5Ni_{2.5}O_x$; (7)$Ce_{20}Cu_5Ni_5O_x$.

The band at 462 cm^{-1} ascribed to cubic CeO_2 that appeared in the visible spectra was shifted for the other samples. A similar phenomenon was observed for the UV Raman spectra. This also indicated the formation of a solid solution. We can deduce that Cu-Ce-Ni-O was formed in the $Ce_{20}Cu_5Ni_{0.4}O_x$ sample. That is, the $Ce_{20}Cu_5Ni_{0.4}O_x$ catalyst was in the form of an imperfect face centered cubic structure, which caused the distortion of the lattice and increased oxygen vacancies, thus enhancing the dynamic oxygen storage and release performance of the catalyst.

3.4. XPS results

In order to further characterize the surface composition and chemical state of the elements on the catalyst surface, X-ray photoelectron spectroscopy was carried out. The Cu 2*p*, O 1*s*, and Ce 3*d* XPS and Cu LMM Auger spectra of the three samples $Ce_{20}Cu_5O_x$, $Ce_{20}Cu_5Ni_{0.4}O_x$, and $Ce_{20}Cu_5Ni_5O_x$ are presented in Fig. 5. The Cu 2*p* XPS spectra of the three catalysts in Fig. 5(a) showed two main peaks at 933.9 and 953.8 eV for Cu $2p_{3/2}$ and Cu $2p_{1/2}$, respectively. According to the literatures [35–37], a binding energy of Cu^{2+} of CuO of 934.0 eV and a shake-up satellite feature in the range of 940–950 eV are characteristic of CuO. In addition, the binding energy of either Cu^{+} or Cu^{0} is near 933.0 eV and no satellite peak exists in the region of 940–950 eV. It was reported that Cu^{2+} exhibits satellite peaks while Cu^{+} does not [38,39]. The lower Cu 2*p* binding energy (933.9 eV) and the absence of a shake-up satellite structure suggested that a small amount of copper clusters was present on the surface together with reduced copper species. This indicated the presence of Cu^{2+}, Cu^{+}, or Cu^{0} in the three catalysts.

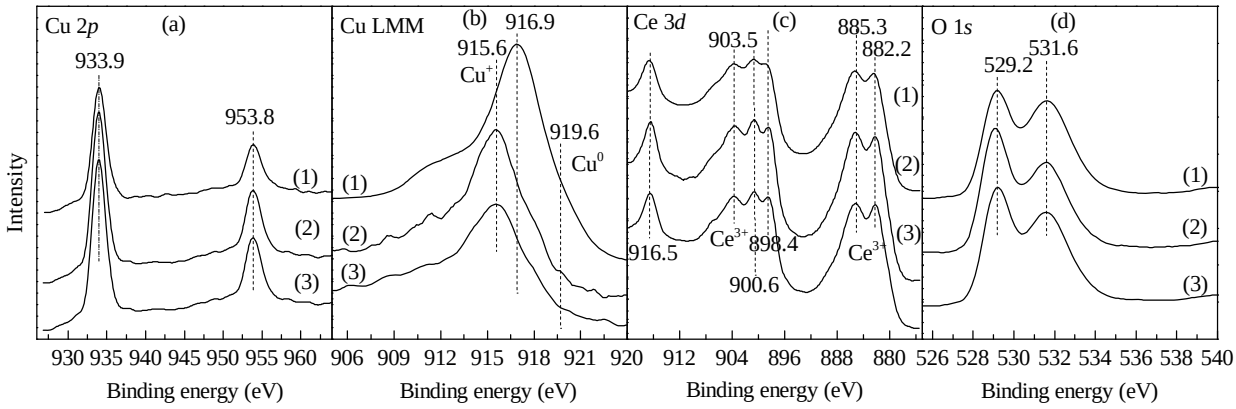

Fig. 5. Cu 2*p* (a), Cu LMM (b), Ce 3*d* (C), and O 1*s* (d) XPS spectra of the catalysts. (1) $Ce_{20}Cu_5O_x$; (2) $Ce_{20}Cu_5Ni_{0.4}O_x$; (3) $Ce_{20}Cu_5Ni_5O_x$.

It is difficult to distinguish between Cu^+ and Cu^0 on the basis of the Cu $2p_{3/2}$ binding energies alone because they are essentially identical. The Cu LMM Auger lines can be used to solve this problem. In Fig. 5(b), it can be observed that the Cu LMM Auger spectrum had a broad feature centered at 916.9 eV for the $Ce_{20}Cu_5O_x$ sample, indicating the presence of both Cu^{2+} and Cu^+ species on the catalyst surface [36]. For the other catalysts with added Ni, the Cu LMM Auger spectra had a broad feature at 915.6 eV, indicating that large quantities of the Cu^+ species existed on the $Ce_{20}Cu_5Ni_{0.4}O_x$ and $Ce_{20}Cu_5Ni_5O_x$ catalyst surface [35,37]. In addition, we only observed a peak at 919.6 eV from $Ce_{20}Cu_5Ni_{0.4}O_x$, which can be assigned to Cu^0 [36,37]. Liu and Flytzani-Stephanopoulos [1] have proposed that a Cu^+ species resulted from the strong interaction of a copper oxide cluster with cerium oxide. The formation of Cu^+ might be induced by the substitution between the two oxide phases at the interface because of the similarity of the Ce^{4+} and Cu^+ ionic radii. The presence of large quantities of the Cu^+ species in the $Ce_{20}Cu_5Ni_{0.4}O_x$ and $Ce_{20}Cu_5Ni_5O_x$ catalysts suggested a synergistic interaction among Ni-O, Cu-O, and Ce-O. This interfacial metal oxide-support synergistic effect may be the reason for the formation of Cu^+ and Cu^0 in the fresh $Ce_{20}Cu_5Ni_{0.4}O_x$ catalyst. In addition, it is known that Cu^+ can enter the CeO_2 lattice to form a solid solution. So we can deduce that the Cu^+ is a copper species dissolved in the CeO_2 lattice and a Cu-O-Ce solid solution was formed in $Ce_{20}Cu_5Ni_{0.4}O_x$, which agreed with the Raman results.

Figure 5(c) shows the Ce 3*d* XPS spectra from the three samples. These are very complicated due to the overlap of the spectra from the Ce^{4+} and Ce^{3+} components. The Ce 3*d* spectrum consists of six peaks at 916.5, 903.5, 900.6, 898.4, 885.3, and 882.2 eV for CeO_2 from the Ce 3*d* level, which can be ascribed to three pairs of spin-orbit doublets ($3d_{3/2}$ and $3d_{5/2}$). By comparison with data reported in the literature [40], we can assign the principal peaks of Ce $3d_{3/2}$ and Ce $3d_{5/2}$ to the peaks at 898.4 and 882.2 eV, respectively, which are from the electron configurations of $3d^94f^0$ and $3d^94f^2$ of Ce^{4+}. The peak at 916.3 eV ($3d^{10}4f^0$ state of Ce^{4+}) can be ascribed to Ce^{4+}. It was reported [41] that the peak at 900.6 eV was due to Ce $3d_{3/2}$ ionization. In the literature [29,36], there are two peaks at 889.9 and 907.5 eV, which are assigned to the state of Ce(IV). However, no peaks at 889.9 and 907.5 eV were found in Fig. 5(c). Instead, strong peaks at 885.3 and 903.5 eV, which are the characteristic peaks of Ce_2O_3, were found. Normally the peaks at 885.3 and 903.5 eV that are ascribed to Ce^{3+} do not appear for the CuO/CeO_2 catalysts. These peaks were observed clearly when the catalyst was reduced with hydrogen or after the reaction [29]. The presence of a large amount of Ce^{3+} may be partly attributed to the formation of a relative homogeneous Cu-Ce-O solid solution because its Cu and Ce atoms facilitate the valence change of Ce ($Ce^{4+} \rightarrow Ce^{3+}$). Another cause would be the substitution of Cu^{2+} for Ce^{4+} in the CeO_2 lattice and the spontaneous transformation of the Ce^{4+} ion (r_{Ce4+} = 0.092 nm) into the larger Ce^{3+} (r_{Ce3+} = 0.103 nm), making this substitution easier. Additionally, it was observed that the intensity of the Ce 3*d* signal for the $Ce_{20}Cu_5Ni_{0.4}O_x$ catalyst was stronger than that from the $Ce_{20}Cu_5O_x$ sample and the intensities of the peaks corresponding to Ce^{3+} were also increased. Moreover, it can be seen that the stronger peaks (885.3 and 903.5 eV) can be ascribed to the Ce^{3+} of the $Ce_{20}Cu_5Ni_{0.4}O_x$ and $Ce_{20}Cu_5Ni_5O_x$ catalysts, leading to the broadening and slight shifting of the Ce $3d_{5/2}$ peak. This observation suggested that the presence of a large amount of Ce^{3+} was due to the presence of NiO.

From the Ce 3*d* XPS spectra, it is apparent that a large amount of Ce present in these samples existed in +3 oxidation state. The generation of both the Ce^{3+} and Cu^+ species (in Fig. 5(a) and (b)) is based on the redox equilibrium ($Ce^{4+} + Cu^+ \leftrightarrow Ce^{3+} + Cu^{2+}$) during the calcination process in the catalyst preparation. This has been claimed to be the source of a synergistic effect on catalytic properties [42]. We can deduce that Cu^+ and Ce^{3+} were stabilized in the catalyst due to the formation of the solid solution. Due to the similarity of the ion radii of Cu^+ (r_{Cu+} = 0.096 nm), Ce^{3+} (r_{Ce3+} = 0.0103 nm) and Ce^{4+} (r_{Ce4+} = 0.092 nm), which have the same face centered cubic crystal structure with an octahedral coordination environment [29], Cu^+ can easily enter the CeO_2 lattice.

In Fig. 5(d), the peak at 529.2 eV can be assigned to lattice oxygen in the metal oxides [43], while the peak at 531.6 eV can be ascribed to adsorbed oxygen or oxygen in hydroxyl groups (adsorbed H_2O, CO_2, surface –OH). It can be observed that the shoulder peak at 529.1 eV from $Ce_{20}Cu_5Ni_{0.4}O_x$ was much higher than those from the other two catalysts, while the intensity

of the peak at 531.6 eV for $Ce_{20}Cu_5Ni_{0.4}O_x$ was the weakest among the three samples. This suggested that adsorbed oxygen can be transformed into lattice oxygen by the introduction of NiO, thus promoting the catalytic activity. It is well known that lattice oxygen plays a key role in CO oxidation. The increased amount of lattice oxygen indicated the production of more oxygen vacancies, which improves the ability of activating and transferring oxygen, therefore facilitating the catalytic reaction. This would be due to the presence of Cu^+ and Ce^{3+} in the catalyst, which favor the formation of oxygen vacancies in the oxide surface. The mechanism of CO oxidation on metal oxides is the following: (1) $CO + O_{lattice} \rightarrow CO_2 + O_{vacan}$, (2) $O_2 + 2O_{vacan} \rightarrow 2O_{lattice}$ [44]. The oxidation rate depends on the controlling step of the redox reaction. Therefore, the increase of lattice oxygen is favorable for the oxidation of CO.

3.5. H_2-TPR results

The active species for CO oxidation are the reducible metals on the surface of the catalysts. To investigate the reducibility of the catalysts, H_2-TPR experiments were performed. Figure 6 shows the H_2-TPR profiles of the $Ce_{20}Cu_5Ni_yO_x$ catalysts with added nickel. For the $Ce_{20}Cu_5O_x$ catalyst, two reduction peaks at 203 and 226 °C were observed. The $Ce_{20}Cu_5Ni_5O_x$ catalyst showed a peak at 230 °C with a low temperature shoulder peak (about 200 °C). Two reduction peaks were also found in the H_2-TPR profile of the $Ce_{20}Cu_5Ni_{0.4}O_x$ catalysts, but the reduction temperatures were lower than those of the $Ce_{20}Cu_5O_x$ catalyst. These were at 185 and 212 °C. Based on the structure characterization results, it can be suggested that a solid solution was formed in the $Ce_{20}Cu_5Ni_{0.4}O_x$ catalyst. From the literature [29], we can deduce that the oxygen vacancies of the $Ce_{20}Cu_5Ni_{0.4}O_x$ solid solution and adsorbed oxygen from the surrounding can be reduced at lower temperatures. Therefore, the peak at 185 °C can be ascribed to the reduction of these oxygen species. The peak at 212 °C was due to the reduction of CuO and partial reduction of CeO_2. These results imply that the addition of Ni enhanced the redox properties of the $Ce_{20}Cu_5O_x$ catalyst. The enhanced redox properties was because the formation of a solid solution with oxygen vacancies not only decreased the reduction temperature but also promoted the mobility of bulk oxygen which is beneficial for the CO oxidation reaction.

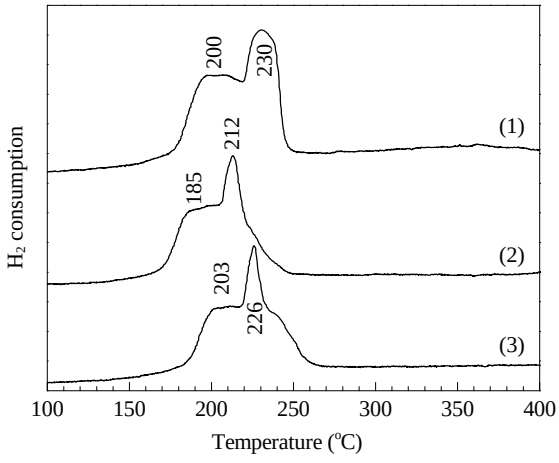

Fig. 6. H_2-TPR profiles of the catalysts. (1) $Ce_{20}Cu_5O_x$; (2) $Ce_{20}Cu_5Ni_{0.4}O_x$; (3) $Ce_{20}Cu_5Ni_5O_x$.

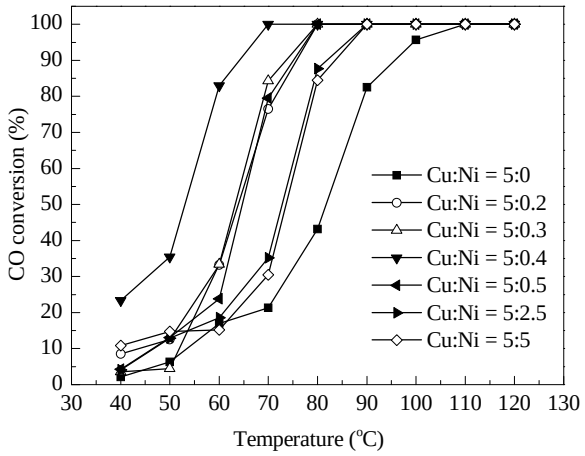

Fig. 7. Activity of the $Ce_{20}Cu_5Ni_yO_x$ catalysts for CO oxidation under the experimental conditions of molar ratio O_2/CO = 1:1, 1 vol% CO.

3.6. Catalytic performance of the catalysts for CO oxidation

The catalytic activities of the $Ce_{20}Cu_5Ni_yO_x$ catalysts with added nickel for CO oxidation as a function of reaction temperature are shown in Fig. 7. The $Ce_{20}Cu_5O_x$ sample exhibited poor catalytic performance for CO oxidation in comparison with the other catalysts, and showed complete CO conversion at 110 °C. It can be observed that the addition of a small amount of Ni led to a large increase in the catalytic activity for the reaction at low temperature. With increasing nickel content, the catalytic activity was initially increased and attained a maximum when the Cu/Ni atomic ratio was 5:0.4. However, with a further increase in nickel content, the catalytic activity decreased. The $Ce_{20}Cu_5Ni_{0.4}O_x$ catalyst presented the highest catalytic activity for CO oxidation. Its temperature at which the complete oxidation of CO occurred was lower than those for the other catalysts, and it showed complete CO conversion at 70 °C. Kim and Cha [18] reported that a 8 wt% CuO/CeO_2 catalyst gave the highest CO conversion (> 99%) under the experimental conditions of molar ratio O_2/CO = 1:1, 1 vol% CO, and 120–190 °C. Sirichalprasert et al. [45] reported that a α-Fe_2O_3-promoted Cu-Ce-O catalysts pretreated with oxygen exhibited a better catalytic performance at 115 °C with 50% CO conversion. Park et al. [46] demonstrated that the catalytic activity of a $CuO\text{-}CeO_2/\gamma\text{-}Al_2O_3$ catalyst for CO oxidation was significantly improved by the addition of a small amount of Co, and it showed complete CO conversion at 155 °C. It was found that the Co added to the Cu-Ce catalyst facilitated the formation of the active Cu species. Li et al. [47] studied the influence of added Mn on the performance of the $CuO\text{-}CeO_2$ catalyst and showed that the catalyst exhibited high catalytic activity for CO oxidation at 120 °C with 99.8% CO conversion. In the literature, the temperature at which CO was oxidized completely is higher than 110 °C for the Cu-Ce based catalysts. The addition of nickel reduced significantly the reaction temperature at which the complete oxidation of CO was reached.

From the Raman results (based on the area of the peak from oxygen vacancies in the UV Raman spectra), the amount of Cu-O-Ce solid solution in the catalysts increased as follows: $Ce_{20}Cu_5Ni_{0.4}O_x$ > $Ce_{20}Cu_5Ni_5O_x$ > $Ce_{20}Cu_5O_x$, which is the order of the activity, indicating that the catalytic activity is related to the solid solution structure.

For the Cu-Ce catalyst system, the interaction and synergism between copper nanoparticles and the ceria support, as well as the activating action of the $Ce^{4+} + Cu^{+} \rightarrow Ce^{3+} + Cu^{2+}$ pairs [44,48] play very important roles. The XPS results showed large amounts of Cu^{+} and Ce^{+3} existing in the $Ce_{20}Cu_5Ni_{0.4}O_x$ catalyst, suggesting that Cu^{+} and Ce^{3+} were stabilized in the catalyst. Moreover, a synergistic function between Cu^{2+}/Cu^{+} and Ce^{4+}/Ce^{3+} was found in the redox cycle. The results imply that the addition of Ni enhanced the interaction and synergism between copper oxide nanoparticles and ceria. This modification is beneficial for the CO oxidation reaction because it involves electron transfer between the catalyst and the reactants. The presence of Ni in the catalyst favors the segregation of metallic ions to form CuO clusters on the surface of ceria, and it increased ion mobility by the formation of a Ni-O-Ce solid solution and more easily released lattice oxygen. Incorporating Ni^{2+} into cerium oxide promoted the reducibility of Ce^{4+} (Ni^{2+}) to Ce^{3+} (Ni^{+}), enhanced the flexibility of copper ions to adapt the oxidation state of Cu^{+} while maintaining the electronic neutrality of the lattice. The smaller particle size and higher surface area expose more unsaturated coordination sites to gas molecules and thus increased the catalytic activity. Doping NiO into the CuO-CeO_2 catalyst decreased the activation temperature of the Cu^{+}–CO species, which is a key intermediate for CO conversion.

Meanwhile, it is known that when Ce^{4+} in the CeO_2 lattice is replaced by Cu^{2+}, defect centers are created. Doping copper into ceria also promoted the formation of Ce^{3+} ions due to the smaller size of the Cu^{2+} that takes part in releasing the strain associated with the increase of the ionic size accompanying the change of Ce^{4+} to Ce^{3+}. The substitution of Cu^{2+} for Ce^{4+} in the CeO_2 lattice would lead to the creation of oxygen vacancies. Surface oxygen and oxygen vacancies are involved in the catalytic activity, and enhancing oxygen mobility will enable the redox process to occur at lower temperatures**.** The migration of oxygen on the surface of the catalysts plays a very important role for CO oxidation. For the $Ce_{20}Cu_5Ni_{0.4}O_x$ catalyst, the formation of the Ni-O-Ce solid solution increased ion mobility, leading to more Cu-O-Ce solid solution being formed. Therefore, oxygen vacancies were created and a higher activity achieved.

4. Conclusions

The $Ce_{20}Cu_5Ni_{0.4}O_x$ catalyst was the most active of the NiO-promoted CuO-CeO_2 catalysts prepared in the present work for CO oxidation at low temperature. XPS characterization showed that large amounts of Cu^{+} and Ce^{3+} existed in the fresh catalysts. Raman results showed a large amount of oxygen vacancies from the generation of Ce^{4+}/Ce^{3+} couples and active oxygen species in the $Ce_{20}Cu_5Ni_{0.4}O_x$ catalyst. These results indicated the formation of a solid solution of Cu-O-Ce. The introduction of NiO increased the BET surface area of the catalyst, increased the dispersion of CuO on CeO_2, and gave more isolated Cu^{2+} in the octahedral sites of CeO_2. The addition of NiO also led to the generation of more oxygen vacancies in ceria by the formation of a Ni-O-Ce solid solution. Moreover, the formation of surface Cu^{+} indicated a strong interaction among Cu, Ni, and Ce, which improved the reducibility of CuO. The high catalytic activity of the catalyst was mainly due to Cu^{+} in the catalyst and the formation of solid solutions of both Cu-O-Ce and Ni-O-Ce.

References

[1] Liu W, Flytzani-Stephanopoulos M. *J Catal*, 1995, 153: 304
[2] Zheng X C, Zhang X L, Wang X Y, Wang S R, Wu S H. *Appl Catal A*, 2005, 295: 142
[3] Luo M F, Ma J M, Lu J Q, Song Y P, Wang Y J. *J Catal*, 2007, 246: 52
[4] Hoflund G B, Gardner S D, Schryer D R, Upchurch B T, Kielin E J. *Appl Catal B*, 1995, 6: 117
[5] Gokhale A A, Dumesic J A, Mavrikakis M. *J Am Chem Soc*, 2008, 130: 1402
[6] Wang L L, Yang L M, Zhang Y H, Ding W, Chen S P, Fang W P, Yang Y Q. *Fuel Process Technol*, 2010, 91: 723
[7] Sedmak G, Hocevar S, Levec J. *J Catal*, 2003, 213: 135
[8] Wang J B, Tsai D H, Huang T J. *J Catal*, 2002, 208: 370
[9] Ayastuy J L, Gurbani A, González-Marcos M P, Gutiérrez- Ortiz M A. *Ind Eng Chem Res*, 2009, 48: 5633
[10] Zhang H L, Ren L H, Lu A H, Li W C. *Chin J Catal* (张慧丽, 任丽会, 陆安慧, 李文翠. 催化学报), 2012, 33: 1125
[11] Benjaram M R, Gode Thrimurthulu, Katta Lakshmi. *Chin J Catal* (催化学报), 2011, 32: 800
[12] Li Q L, Zhang Y H, Chen G X, Fan J Q, Lan H Q, Yang Y Q. *J Catal*, 2010, 273: 167
[13] Dobrosz-Gómez I, Kocemba I, Rynkowski J M. *Appl Catal B*, 2008, 83: 240
[14] Jiang X Y, Zhou R X, Pan P, Zhu B, Yuan X X, Zheng X M. *Appl Catal A*, 1997, 150: 131
[15] Liu Y, Fu Q, Stephanopoulos M F. *Catal Today*, 2004, 93-95: 241
[16] Skårman B, Grandjean D, Benfield R E, Hinz A, Anderson A, Wallenberg L R. *J Catal*, 2002, 211:119
[17] Marbán G, Fuertes A B. *Appl Catal B*, 2005, 57: 43
[18] Kim D H, Cha J E. *Catal Lett*, 2003, 86: 107
[19] Tang X L, Zhang B C, Li Y, Xu Y D, Xin Q, Shen W J. *Catal Today*, 2004, 93-95: 191
[20] Skarman B, Nakayama T, Grandjean D, Benfield R E, Olsson E, Niihara K, Wallenberg L R. *Chem Mater*, 2002, 14: 3686
[21] Zhang R D, Teoh W Y, Amal R, Chen B H, Kaliaguine S. *J Catal*, 2010, 272: 210
[22] Zhang Z L, Zhang Y X, Mu Z G, Yu P F, Ni X Z, Wang S L, Zhang L S. *Appl Catal B*, 2007, 76: 335
[23] Fornasiero P, Fonda E, Di Monte R, Vlaic G, Kaspar J, Graziani M. *J Catal*, 1999,187: 177
[24] Kruk M, Jaroniec M. *Chem Mater*, 2001, 13: 3169
[25] Dow W, Wang Y, Huang T. *Appl Catal A*, 2000, 190: 25
[26] Martínez-Arias A, Cataluña R, Conesa J C, Soria J. *J Phys Chem B*, 1998, 102: 809
[27] Spanier J E, Robinson R D, Zhang F, Chan S W, Herman I P. *Phys Rev B*, 2001, 64: 245407
[28] Shan W J, Feng Z C, Li Z L, Zhang J, Shen W J, Li C. *J Catal*, 2004, 228: 206

Graphical Abstract

Chin. J. Catal., 2013, 34: 322–329 doi: 10.1016/S1872-2067(11)60468-3

Low temperature CO oxidation on Ni-promoted CuO-CeO_2 catalysts

CHEN Guoxing, LI Qiaoling, WEI Yucai, FANG Weiping, YANG Yiquan*
Xiamen University

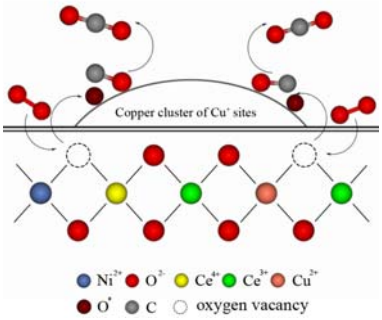

The high catalytic activity of Ni-promoted CuO-CeO_2 is due to the promoter giving increased amounts of Cu^+ in the catalyst and the formation of solid solutions of Cu-O-Ce and Ni-O-Ce.

[29] Bera P, priolkar K R, Sarode P R, Hegde M S, Emura S, Kumashiro R, Lalla N P. *Chem Mater*, 2002, 14: 3591
[30] Liu W H, Li D, Sun K, Li Y S, Fu Z W. *Solid State Sci*, 2009, 11: 982
[31] Martínez-Arias A, Gamarra D, Fernández-García M, Wang X, Hanson J, Rodriguez J. *J Catal*, 2006, 240: 1
[32] McBride J R, Hass K C, Poindexter B D, Weber W H. *J Appl Phys*, 1994, 76: 2435
[33] Yashima M, Arashi H, Kakihana M, Yoshimura M. *J Am Ceram Soc*, 1994, 77: 1067
[34] Wang X, Rodríguez J A, Hanson J C, Gamarra D, Martínez-Arias A, Fernández-García M. *J Phys Chem B*, 2005, 109: 19595
[35] Avgouropoulos G, loannides T. *Appl Catal A*, 2003, 244: 155
[36] Tschöpe A, Trudeau M L, Ying J Y. *J Phys Chem B*, 1999, 103: 8858
[37] Dai W L, Sun Q, Deng J F, Wu D, Sun Y H. *Appl Surf Sci*, 2001, 177: 172
[38] Vepřek S, Cocke D L, Kehl S, Oswald H R. *J Catal*, 1986, 100: 250
[39] Ghijsen J, Tjeng L H, van Elp J, Eskes H, Westerink J, Sawatzky G A, Czyzyk M T. *Phys Rev B*, 1998, 38: 11322
[40] Moretti E, Lenarda M, Storaro L, Talon A, Frattine R, Polizzi S, Castellón E R, Jimenez-López A. *Appl Catal B*, 2007, 72: 149
[41] Nelson A E, Schulz K H. *Appl Surf Sci*, 2003, 210: 206
[42] Polster C S, Nair H, Baertsch C D. *J Catal*, 2009, 266: 308
[43] Avgouropoulos G, loannides T. *Appl Catal B*, 2006, 67: 1
[44] Hocevar S, Batista J, Levec J. *J Catal*, 1999, 184: 39
[45] Sirichaiprasert K, Luengnaruemitchai A, Pongstabodee S. *Int J Hydrogen Energy*, 2007, 32: 915
[46] Park J W, Jeong J H, Yoon W L, Jung H, Lee H T, Lee D K, Park Y K, Rhee Y W. *Appl Catal A*, 2004, 274: 25
[47] Li J, Zhu P F, Zuo S F, Huang Q Q, Zhou R X. *Appl Catal A*, 2010, 381: 261
[48] Liu W, Flytzani-Stephanopoulos M. *Chem Eng J*, 1996, 64: 283

镍促进 CuO-CeO_2 催化剂的结构表征及低温 CO 氧化活性

陈国星[a], 李巧灵[a], 魏育才[a], 方维平[a,b], 杨意泉[a,b,*]
[a]厦门大学化学化工学院化工系, 福建厦门 361005
[b]厦门大学化学化工学院化学系, 醇醚酯清洁生产国家工程实验室, 福建厦门 361005

摘要: 制备了一系列CO低温氧化的$Ce_{20}Cu_5Ni_yO_x$催化剂, 并采用氮气低温物理吸附、X射线衍射、程序升温还原、X射线光电子能谱以及拉曼光谱等手段对催化剂进行表征. 结果表明, $Ce_{20}Cu_5Ni_{0.4}O_x$催化剂活性最高. NiO的添加可以使得较多的Cu物种掺杂到CeO_2晶格中, 通过形成铈镍固溶体产生更多的氧空位. 表征结果显示, $Ce_{20}Cu_5Ni_{0.4}O_x$催化剂中存在大量的Cu^+, Ce^{3+}及晶格氧, 催化剂中的Cu^+很容易进入到氧化铈晶格, 形成Cu-O-Ce固溶体, 从而增强了在还原气氛下晶格氧的释放能力. $Ce_{20}Cu_5Ni_{0.4}O_x$催化剂高的催化活性主要归因于大量Cu^+以及形成的Cu-O-Ce和Ni-O-Ce固溶体.

关键词: 铜; 铈; 一氧化碳; 氧化; 镍; 固溶体

收稿日期: 2012-09-05. 接受日期: 2012-10-11. 出版日期: 2013-02-20.
*通讯联系人. 电话: (0592)2186368; 传真: (0592)2180361; 电子信箱: yyiquan@xmu.edu.cn
基金来源: 福建中烟工业公司.
本文的英文电子版由Elsevier出版社在ScienceDirect上出版(http://www.sciencedirect.com/science/journal/18722067).